STRUCTURAL BIOLOGY

The cryo-EM structure of an ERAD protein channel formed by tetrameric human Derlin-1

Bing Rao[1]*, Shaobai Li[2]*, Deqiang Yao[2]*†, Qian Wang[2], Ying Xia[2], Yi Jia[2], Yafeng Shen[2], Yu Cao[2,3]‡

Endoplasmic reticulum–associated degradation (ERAD) is a process directing misfolded proteins from the ER lumen and membrane to the degradation machinery in the cytosol. A key step in ERAD is the translocation of ER proteins to the cytosol. Derlins are essential for protein translocation in ERAD, but the mechanism remains unclear. Here, we solved the structure of human Derlin-1 by cryo–electron microscopy. The structure shows that Derlin-1 forms a homotetramer that encircles a large tunnel traversing the ER membrane. The tunnel has a diameter of about 12 to 15 angstroms, large enough to allow an α helix to pass through. The structure also shows a lateral gate within the membrane, providing access of transmembrane proteins to the tunnel, and thus, human Derlin-1 forms a protein channel for translocation of misfolded proteins. Our structure is different from the monomeric yeast Derlin structure previously reported, which forms a semichannel with another protein.

INTRODUCTION

The endoplasmic reticulum (ER) serves as a checkpoint for protein folding and posttranslational modifications. Efficient cleanup of misfolded proteins is important for ER homeostasis, and a complex molecular pathway, ER-associated degradation (ERAD), plays a major role in the elimination of these ER-retained proteins (*1*). Deficiencies in ERAD cause accumulation of misfolded proteins and lead to diseases such as cystic fibrosis and inclusion body myopathy (*2*–*4*). An important step in ERAD is the transportation of misfolded proteins from the ER lumen or membrane into the cytosol, a process known as retrotranslocation (*5*). The ERAD retrotranslocation is poorly understood, and the mechanism of protein translocation remains unknown. Even the proteins that are directly involved in protein translocation are not clear. Candidate proteins include the Sec61 complex (*6*), Hrd1-Hrd3 complex (*7*), Derlin family members (*8*, *9*), and Hrd1-Der1 complex (*10*).

The Derlin family belongs to the rhomboid superfamily and consists of three member genes in the human genome, Derlin-1, Derlin-2, and Derlin-3 (*11*, *12*). Sequence-based prediction and previous studies in biochemistry/structural biology indicated that they are multipass membrane proteins with four to six transmembrane (TM) helices and both N and C termini residing in the cytosol (*10*, *12*–*14*). Human Derlins are essential for the degradation of both secretory and membrane proteins in ERAD, such as class I major histocompatibility complex (MHC-I), α-1 antitrypsin, and cystic fibrosis TM conductance regulator (CFTR) (*8*, *9*, *12*, *15*). There are two Derlin homologs in *Saccharomyces cerevisiae*, Der1 and Dfm1 (*16*, *17*). Although yeast Der1 was studied more extensively in the structure-function relationship of ERAD, mammalian Derlin proteins share more similarity to Dfm1, since they have a small heterodimer partner (SHP) box at the C-terminal domain serving as a Cdc48p/Valosin-containing protein (VCP)–binding motif (*13*, *18*), which is absent in yeast Der1. The existence of this motif implies that an alternative mechanism might exist for the mammalian Derlin-mediated and yeast Dfm1-mediated ER retrotranslocation (*19*, *20*). Here, we purified the human Derlin-1 (hDERL1) protein as a homotetramer and solved its structure by cryo–electron microscopy (cryo-EM). The structure of hDERL1 reveals a tunnel in the center of the Derlin tetramer, large enough to allow passage of α-helical peptide across the ER membrane. The structure of hDERL1 demonstrates a retrotranslocation channel in ERAD.

RESULTS

The electron microscopic analysis on hDERL1

Unlike the monomeric form of yeast Der1 in the cryo-EM structure as in the yeast Hrd1 ubiquitin ligase complex (*10*), hDERL1 was reported to form homo-oligomer in an immunoprecipitation assay (*21*), which is supported by the in-membrane cross-linking assay on membrane fractions from human embryonic kidney (HEK) 293T cells overexpressing hDERL1 (fig. S7). To obtain detailed insights into the structure of hDERL1, we expressed the full-length hDERL1 with a C-terminal twin-strep tag in Expi293F cells. The protein was solubilized with lauryl maltose neopentyl glycol (LMNG) and further purified by size-exclusion chromatography in glyco-diosgenin (GDN) (fig. S2). Cryo-EM images of purified sample were collected using a Titan Krios transmission electron microscope (FEI) operated at 300 kV, and data processing was performed using RELION-3 and cryoSPARC. Both two-dimensional (2D) and 3D classification on the hDERL1 particles confirmed that hDERL1 forms a homotetramer. Initial efforts on 3D refinement using C4 symmetry resulted in a structural model at an overall resolution of 4.4 Å. However, further examination of the 2D images revealed that a twofold, rather than fourfold, symmetry might apply to the hDERL1 tetramer particles (fig. S2), and this was confirmed by the subsequent 3D refinement with C2 symmetry setup, which generated maps at an overall resolution of 3.8 Å (Fig. 1A, fig. S3, and Table 1). Further 3D refinement iteration was conducted using C1 symmetry but resulted in an electron

[1]CAS Center for Excellence in Molecular Cell Science, Shanghai Institute of Biochemistry and Cell Biology, Chinese Academy of Sciences, University of Chinese Academy of Sciences, 333 Haike Road, Shanghai 201210, China. [2]Shanghai Institute of Precision of Medicine, Shanghai Ninth People's Hospital, Shanghai Jiao Tong University School of Medicine, 115 Jinzun Road, Shanghai 200125, China. [3]Department of Orthopaedics, Shanghai Key Laboratory of Orthopaedic Implant, Shanghai Ninth People's Hospital, Shanghai Jiao Tong University School of Medicine, Shanghai 200011, China.
*These authors contributed equally to this work.
†Present address: iHuman Institute, ShanghaiTech University, Shanghai 201210, China.
‡Corresponding author. Email: yu.cao@shsmu.edu.cn

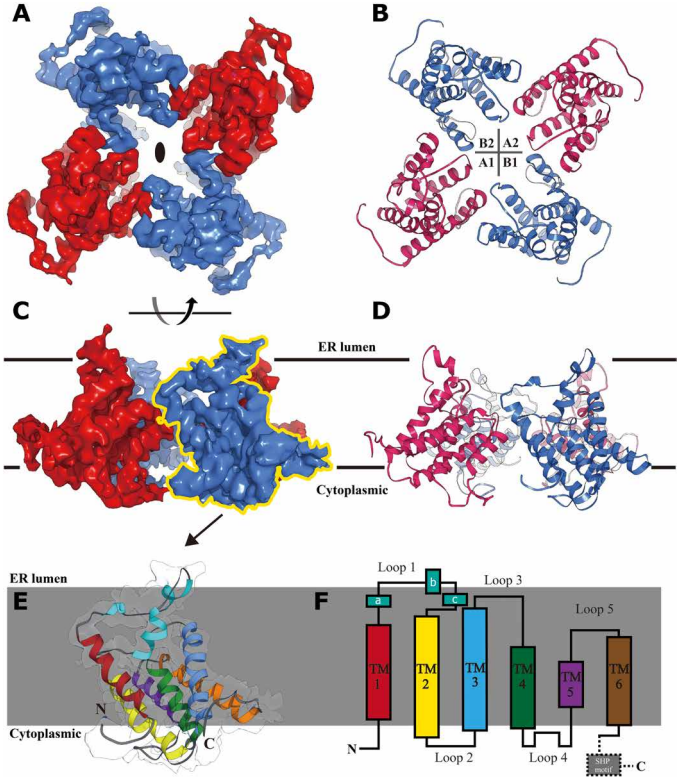

Fig. 1. hDERL1 forms tetrameric channels with C2 symmetry. (**A** and **B**) hDERL1 cryo-EM map and molecular model viewed from the lumen side of the ER membrane, respectively. The four hDERL1 molecules in the C2 tetramer adapt into two conformations, A (in red) and B (in blue), and, thus, were designated as Mol. A1, Mol. A2, Mol. B1, and Mol. B2, respectively. (**C** and **D**) hDERL1 cryo-EM map and molecular model viewed parallel to the ER membrane. (**E**) Side view of molecular model for Mol. B1 colored by TM helices and fit in map segment from (C). (**F**) Cartoon representation of hDERL1 monomer topology. The TM helices 1 to 6; lumenal helices a, b, and c were colored according to the same scheme as in (E). The cell membrane was shown as gray block, and the orientation was labeled according to the calculation using the PPM server (https://opm.phar.umich.edu/ppm_server). The unsolved C-terminal loop and SHP motif were shown in dashed lines and frame. All structure graphs in this and following figures were generated with PyMOL (the PyMOL Molecular Graphics System, version 1.9, Schrödinger, LLC.) and UCSF Chimera [the University of California, San Francisco (UCSF) Resource for Biocomputing, Visualization, and Informatics, version 1.13.1] (*48*).

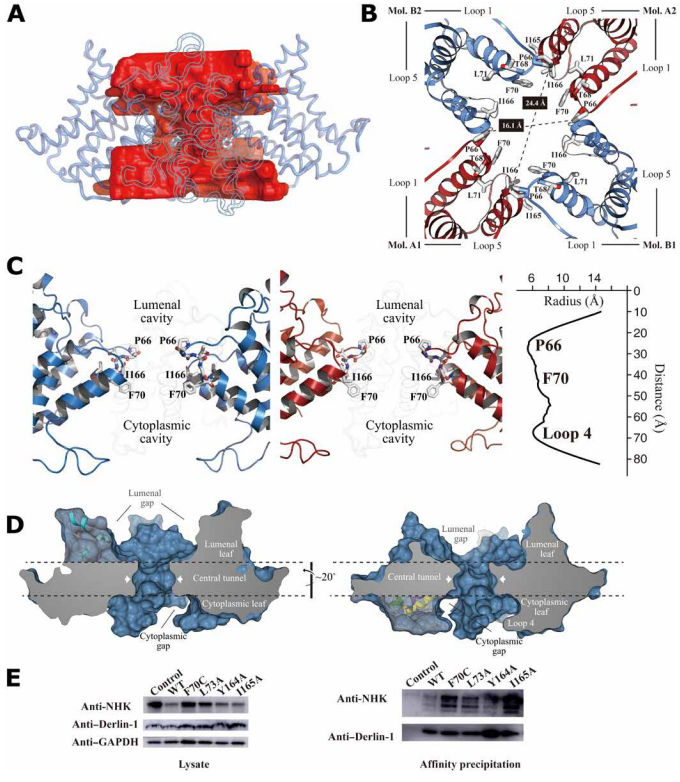

Fig. 2. The TM pathway in Derlin-1 channel. (**A**) The permeation pathway formed by tetrameric hDERL1, as determined by HOLE (*22*), is shown in the red surface in a cartoon representation of hDERL1 with the protomer close to observers shown as transparent model. (**B**) The intersecting surface of the central tunnel of hDERL1 viewed from the lumen side of the ER membrane. The critical residues at the central tunnel and the interface between protomers are shown in a stick model rendered by elements. The distances between P66 residues at diagonal were measured are and shown in dashed lines. (**C**) The intersecting surface of the central tunnel of hDERL1 viewed parallel to the ER membrane at two angles, with the radius for inner pathway calculated by HOLE (*22*) shown in the right panel. The Mol. A1 and Mol. B1 were removed for a clear observation in left and middle panels, respectively. (**D**) The substructure in hDERL1 channel. The hDERL1 tetramer is shown in a surface model and sliced perpendicular to the membrane surface. Part of the cap of clipping surfaces was set to transparent to show the composition of lumenal leaf and cytoplasmic leaf. (**E**) NHK dislocation by hDERL1. Left: Immunoblot of lysates of cells expressing NHK (control) and coexpressing NHK with hDERL1-strep [wild type (WT) and mutants]. Right: Immunoblots of Strep-Tactin magnetic beads precipitated material from cells expressing NHK (control) and coexpressing NHK with hDERL1-strep (wild type and mutants).

density map with notably lower resolution and similar overall shape compared with the map with C2 symmetry (fig. S3). The molecular model for hDERL1 was thus built using the cryo-EM map of C2 symmetry, and each Derlin channel is composed of four hDERL1 molecules in two conformations [molecule A (Mol. A) and Mol. B; Figs. 1B, 2B, and 3B]. Residues 9 to 198 were resolved in each protomer. Residues 193 to 201 were built as polyalanine (fig. S4). Although Derlin-1 forms a homotetramer, neighboring protomers have a slight conformational change that renders the tetramer with C2 symmetry (Figs. 1B and 2B).

The overall architecture of hDERL1 channel

The overall architecture of the tetrameric hDERL1 resembles a Maya temple (Fig. 1, C and D): Lumenal ends of all the TM helices are closer to the center rotational axis at the angels ranging from 40° to 65°. The central tunnel is lined by TM1, TM2, TM5, and loops 1 and 5. The tunnel has a wide opening facing the cytoplasm and a relatively narrow one facing with ER lumen. The region between residues P66 and F70 is constricted, with the narrowest part of the tunnel located at residue P66 that forms constriction with a dimension of about 12 Å by 18 Å in short and long axis as determined by program HOLE (Fig. 2C) (*22*). Leading to the narrowest constriction is two large cavities at both the lumenal and cytoplasmic sides. Neither the lumenal nor cytoplasmic cavity is fully enclosed at its membrane-facing surface, and they branch out as a four-leaf structure, respectively (Fig. 2, A and C). The lumenal leaves of hDERL1 are formed by loop 1, a long stretch of residues conserved in the rhomboid protease family, while at the cytoplasmic side, the leaves are mostly formed by the outwardly tilted TM bundles, especially TM4, TM5, and loop 4 (Fig. 2D). The tunnel would allow passage of peptide chains in α

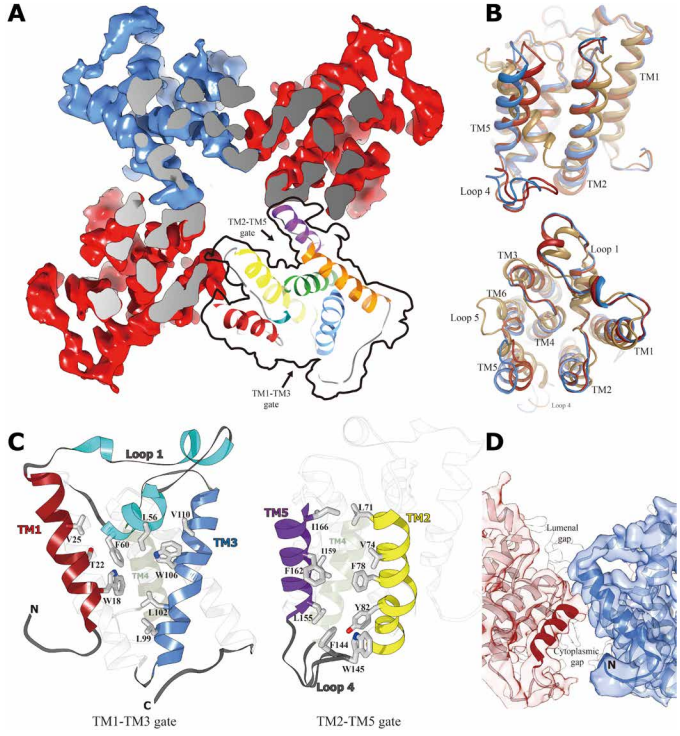

Fig. 3. The lateral gates and gaps on the Derlin-1 tetramer. (**A**) The EM map of hDERL1 was sliced parallel to the membrane surface and is viewed from lumen side of the ER membrane. The clefts on the inner and outer surface of tetrameric ring are indicated with arrows; they formed TM2-TM5 and TM1-TM3 gates. (**B**) The superposition among the structural models of hDERL1 Mol. A (in red), hDERL1 Mol. B (in blue), and yeast Der1 [in brown, edited from coordinate file with Protein Data Bank (PDB) ID 6VJZ]. (**C**) Detailed cartoon representation of TM1-TM3 gate (left) and TM2-TM5 gate (right). The TM helices and loops were colored according to the same scheme as in Fig. 1E, and the residues lining along the gates are shown in stick models rendered by elements. (**D**) A close view to the lumenal gap between loop 1 from neighboring hDERL1 protomers and the cytoplasmic gap, which is partially covered by N-terminal loop.

helix, which range from about 5 to 15 Å in diameter, depending on the side chains, indicating that unfolding of the secondary structure is not required for substrate translocation in ERAD.

The tetrameric hDERL1 ring with C2 symmetry

Although it is unexpected to find a C2 symmetry on the tetrameric ring of hDERL1s, a higher oligomer with lower symmetry is precedented in other studies. For example, glycerol aquaporin AQP10 and AQP7 were reported to form a homotetramer, but both have slightly different conformations among the protomers in the tetramer (*23*, *24*). hDERL1 tetramer is primarily maintained by the interactions between loops 5 and 1 from neighboring protomers, and very limited interactions were identified on the TM helices between protomers (Fig. 2B), implying a loose channel ready to adapt its shape to the substrates of different sizes (fig. S4). The flexibility of the interface loops could not only adjust their local conformation to stretch the intersection shape of the central tunnel, thereby allowing the passage of peptides with large secondary structures and bulky side chains, but also lower the local resolutions of the EM map. Lacking the fourfold symmetry, the Derlin channel forms a central tunnel with a diamond-shaped cross section (Fig. 2B) with a length of about 20 Å (Fig. 2C) along the C2 symmetry axis.

To further explore the role of tetramerization of hDERL1 in its retrotranslocation activities, we conducted an ERAD processing assay using the null Hong Kong variant (NHK), a truncated fragment of α-1 antitrypsin as an established ERAD substrate (*12*). The cells showed a strong overexpression when transiently transfected with complementary DNA (cDNA) of NHK, and the coexpression of NHK with wild-type hDERL1 resulted in a decreased accumulation of NHK as determined by Western blotting, indicating an efficient cleanup by ERAD. When coexpressed with hDERL1 with mutations at the tetrameric interface, the NHK levels in the cells were substantially higher than that with wild type, implying that the cleanup capacity of Derlin-1 was impaired, while their expression levels remained similar to the wild-type Derlin-1 (Fig. 2E). Further analysis using coprecipitation upon NHK with Derlin-1 variants showed that the binding between Derlin-1 and NHK was enhanced, instead of disrupted, by mutations, which indicated that the hDERL1 interface mutations could maintain their ability to recognize and capture NHK but failed to conduct its TM transport.

The lateral gates on the hDERL1 channel

The structure shows hDERL1 in two conformations that we define as Mol. A and Mol. B. A superposition of Mol. A and Mol. B and yeast Der1 is shown in Fig. 3B. The TMs and loops are similar except for TM5 and loop 5: TM5 in both conformations from hDERL1 was largely parallel to TM2 to form a lateral gate between the core of hDERL1 and the central tunnel, resembling the open state of *Escherichia coli* GlpG (ecGlpG), while the TM5 in yeast Der1 titled toward TM2 at the cytoplasmic side to form a closed conformation as shown in the structure of *Haemophilus influenzae* GlpG (hiGlpG) (*10*, *25*, *26*). In hDERL1 tetramer, the TM2-TM5 gates from four protomers are located at the inner side of the channel, and Mol. B opens its TM2-TM5 gate more widely than Mol. A or ecGlpG does (fig. S1). Loop 5 between TM5 and TM6 was proposed as a blocker, covering the TM2-TM5 gate in ecGlpG and hiGlpG, but loop 5 in either human or yeast Derlin is too short to take this role. Instead, in hDERL1, loop 4 between TM4 and TM5 is much longer than other rhomboid proteins, which extends into the bottom of the cytoplasmic cavity underneath the central tunnel, partially sealing the cytoplasmic end of TM2-TM5 cleft with the bulky side chains from W144 and F145 (Fig. 3C).

At the outer side of the Derlin-1 channel, another lateral gate was identified, composing of TM1, TM3, and loop 1 between TM1 and TM2 (Fig. 3, B and C). At the lumenal side, the leaf of loop 1 is half-embedded in the lipidic bilayer and positioned in front of the large cleft between TM1 and TM3. A long-stretched loop 1 sandwiched by TM1 and TM3 helices is a typical feature in the rhomboid protease family and was once proposed as the entrance for the substrate to enter the catalytic core of GlpG (*27*) but then had this role taken by the TM2-TM5 gate based on subsequent mutations and structural analysis (*25*, *28*, *29*). In our tetrameric structure, the four TM1-TM3 gates face the surrounding lipidic environment and, thus, might serve as the entrances for the ERAD targets, such as an integral membrane protein with TM helices. Both the TM1-TM3 and TM2-TM5 gates in hDERL1 are decorated with a series of hydrophobic residues such as W18, V25, L56, F60, L99, L102, and W106 in TM1-TM3 gate and L71, V74, F78, Y82, L155, I159, and F162 in TM2-TM5 gate (Fig. 3C), mimicking the lipidic environment for a misfolded ER membrane protein substrate (ERAD-M) to facilitate its transition from the membrane-bound state to Derlin-trapped state.

The routine for the retrotranslocation of ERAD substrate

For misfolded proteins embedded in the ER membrane, their access to the central tunnel could be achieved by the opening of the interface between the protomers. As shown in Figs. 2D and 3D, at neither the lumenal nor cytoplasmic side of the hDERL1 tetramer does an enclose channel exist. Instead, two sets of four-gap substructures were observed at both ends, giving the lipid-embedding molecules access to the central tunnel. On the one hand, the lumenal gaps are fully open to the surrounding membrane environment and thereby provide the peripheral proteins access to the central tunnel. On the other hand, the cytoplasmic gaps are gated by the N-terminal domain of hDERL1 (Fig. 3D), which is consisted of residues 1 to 11 protruding from TM1 and blocks the gap near the surface of the membrane, preventing the ERAD substrates from leaving the cytoplasmic cavity freely. Furthermore, four loop 4s pointing to the center of the cytoplasmic cavity might also constrain the substrates, leaving the central tunnel along with a routine close to the center of tetramer (Figs. 2C and 4, inset).

DISCUSSION

Various proteins have been proposed as candidate molecules for translocation channels in previous studies on ERAD such as Sec61, Hrd1, and Derlins. Sec61 complex is known as a peptide channel facilitating newly synthesized peptide chain to enter the ER lumen from the cytosol (*30*) and found involved in the retrotranslocation of some ERAD substrates along the lumen-to-cytosol direction (*31*). However, the protein substrates for Sec61-dependent retrotranslocation are limited, and alternative channels might exist with a more generalized function. Hrd1, also known as Syvn1 in mammals, was first identified as a RING-type ubiquitin E3 ligase, transferring ubiquitin from the E2, Ubiquitin-conjugating enzyme E2 7 (UBC7), to the ERAD substrates extracted from ER and prompting degradation (*32*, *33*). In recent functional studies by Baldridge and Rapoport (*34*), Hrd1 was found to mediate the retrotranslocation of ERAD substrates in vitro, which was further supported by the EM study on Hrd1-Hrd3 complex, showing a half TM tunnel formed by TM3, TM4, TM6, TM7, and TM8 from dimeric Hrd1 (*7*). However, the molecular mechanism for Hrd1-mediated retrotranslocation remains to be elucidated; the energy driving the protein transportation by Hrd1 is unclear since the interaction between Hrd1 and VCP, the major AAA^+ adenosine triphosphatase (ATPase) in ERAD, has not been well established mechanistically. A functional assay using lipid membrane reconstituted with purified Hrd1 shows its autoubiquitination on RING domain could induce an open conformation of Hrd1 and higher affinity to unfolded proteins, implying a retrotranslocation potentially driven by ubiquitination (*35*). The half TM tunnel in the Hrd1 structure requires a relatively substantial conformational change for substrate peptide chain passage, including a series of helix rearrangements and resets, implying slow and energy-consuming transportation conducted by Hrd1. In a recent report by the same group, the structure of a yeast ERAD complex comprising Hrd1, Der1, and Usa1 was determined by cryo-EM, where the yeast Hrd1 binds to Der1 to function as a heterodimer (*10*). The interface between Hrd1-Der1 forms two "half channels," thinning and distorting the local bilayer membrane to allow proteins to travel across the ER membrane. In both the Hrd1 homodimer model and Hrd1-Der1 heterodimer model, there is no substrate conductance pore formed in the retrotranslocation complex, and a detailed mechanism underling the driving force by VCP/p97 for the transportation across the membrane is elusive.

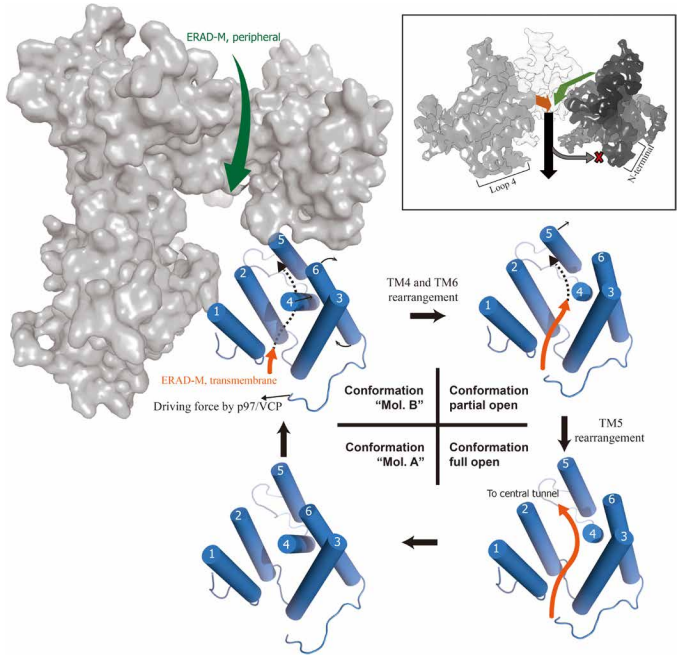

Fig. 4. The mechanistic model for retrotranslocation by Derlin-1 channel. Derlin-1 channel was shown in a mixed model with three hDERL1 protomer in surface model and one as cylinder loop model in four conformations proposed in retrotranslocation. The conformations "Mol. A" and "Mol. B" were solved in the EM structure of hDERL1, while the conformations "partial open" and "full open" were hypothetical states. Inset: The entrance and exit routine of ERAD substrates in our mechanistic model. The cryo-EM map segment for Mol. A1 was removed to show the central tunnel and substructures near to the routine.

One of the biggest challenges in the retrotranslocation of ERAD-M substrates is extracting the TM portion of the substrate proteins from the lipid bilayer, since the hydrophobic interactions between membrane lipids and the lipophilic side chains of ERAD-M substrates make an energy barrier stabilizing them within the ER membrane. Precedent studies provide experimental evidence, indicating that the critical function of Derlin-1 in retrotranslocation and the disruption on hDERL1 expression level will lead to accumulation of ERAD substrates such as CFTR ΔF508 (*15*), MHC-I heavy chain (*8*, *9*), apolipoprotein B (*36*), and sodium channel ENaC (*37*). Although the functional data suggest that hDERL1 is required in substrate recognition and initiation of dislocation, lacking structural model makes it difficult to define a specific role for the Derlin-1 protein in retrotranslocation. Our cryo-EM structure for hDERL1 tetramer implies several important features for it to function as an ERAD-M channel. First, instead of forming a membrane-spanning full-tunnel structure, hDERL1 adapts to a short central tunnel connecting to a large lumenal cavity with gaps laterally open to the lipid environment, allowing the peripheral membrane proteins embedded at the lumenal surface of the ER membrane to enter the central tunnel with no need to reenter the ER lumen first. Second, the two gates at the outer and inner surfaces of Derlin channels, formed respectively by the clefts between TM1-TM3 (outer gate) and TM2-TM5 (inner gate), suggest a potential routine for the TM helices of ERAD-M substrates to travel through the tetrameric ring and enter the central tunnel (Fig. 4). Despite of

the low sequence similarity, both mammalian and yeast Derlin proteins share high homology among their structures, implying common features between intramembrane proteolysis and retrotranslocation of ERAD (*12*), especially a rearrangement within TM helices to allow the access of a proteolysis/dislocation substrate to the center of the rhomboid protein. In rhomboid proteases, the TM2-TM5 gate controls the entrance of substrate to the catalytic triad and the exit of the proteolysis products (*26*, *28*). As observed through the TM1-TM3 and TM2-TM5 gates (Fig. 3C), in the hDERL1 structure, the TM4 sits in the center of the hDERL1 protomer and blocks the passage between the two gates, implying a displacement for TM4 during the retrotranslocation to allow the passage of substrate. In our hDERL1 structure, the two longest loops at lumenal and cytoplasmic sides, loops 1 and 4, were found to partially cover the outer and inner gates, respectively, serving as controlling switches for the pathway from ER membrane to the central tunnel.

The hDERL1-carrying mutations at the tetrameric interface showed a reduced ERAD activity on NHK but a higher binding capacity (Fig. 2E), implying that the impaired tetramerization could block the retrotranslocation at the pretransport state and, thus, result in an accumulation of hDERL1-substrate complex. This supports the transport mechanism we proposed in Fig. 4, which shows that the hDERL1 monomer is the functional unit for substrate capture, while the hDERL1 tetramer functions as the core unit for the TM transport of ERAD substrates.

Direct clues to the molecular mechanism underlying the conformational change during the entrance of ERAD-M into the central tunnel are limited, since the lack of structural information on the C-terminal SHP motif makes it difficult to analyze the interaction between hDERL1 and VCP/p97, the major ATPase and, thus, potential energy supplier in ERAD. Nevertheless, the electron density corresponding to the C terminus of hDERL1 indicates that the unsolved SHP motifs locate underneath the cytoplasmic surface of Derlin-1 tetramer. Previous studies showed that the SHP motif of hDERL1 served as a docking site for VCP/p97 (*8*, *9*, *18*), and, in our retrotranslocation model, the displacement of the N-terminal domain of VCP/p97 upon the adenosine 5′-triphosphate hydrolysis could drive a big movement on SHP motifs, thereby resulting in a conformational change on the C terminus of hDERL1 and, in turn, the rearrangements of hDERL1 TMs to open/close the inner path between the TM1-TM3 and TM2-TM5 gates. In addition to the energy supplier of retrotranslocation, VCP/p97 might also serve as a blocker for the channel, since it could bind to the C-terminal loop of hDERL1 and result in large steric hindrance at the open to the cytoplasmic cavity of Derlin-1 channel, thus preventing ion or small molecule in ER lumen from leaking into the cytosol through the central funnel.

In a summary, the structure of a tetrameric hDERL1 indicates that hDERL1 might form a retrotranslocation channel in ERAD. The difference between the structure of hDERL1 and yeast Der1 might reflect the distinction on their functions in ERAD, and thus, Dfm1, another Derlin ortholog in yeast, might represent an important and underestimated molecule in studying ERAD in yeast model, since Dfm1, in comparison to Der1, resembles human hDERL1 better for its SHP motif and direct interaction with Cdc48, the ortholog for VCP/p97 in yeast. To conduct a continuous and efficient retrotranslocation, Derlin-1 channels might use the ATPase activity of VCP/p97 to power the permeation of ERAD-M substrates, and thus, we expect that a further structural study on the complex between hDERL1 and VCP/p97 would give us more insights into the mechanism of ERAD process.

MATERIALS AND METHODS

Protein purification and expression

The cDNA of human DERL1 (National Center for Biotechnology Information reference sequence: NM_024295.6) was cloned into a modified pcDNA3.4 vector, which contains a PreScission Protease cleavage site and a C-terminal twin strep tag. Expi293F cells (Thermo Fisher Scientific, A14527) were cultured in a chemically defined Union-293 medium (Union-Biotech, UP0050) at 37°C, supplied with 5% CO_2. When cell density reached 2.0×10^6 cells/ml, the cells were transiently transfected with the expression plasmids using PEI MAX (Polysciences), and the transfected cells were cultured for 60 to 72 hours before harvest.

For the purification of Derlin-1, the transfected Expi293F cells were collected and resuspended in lysis buffer containing 25 mM tris (pH 8.0), 150 mM NaCl, 10% glycerol, 10 mM $MgCl_2$, deoxyribonuclease I (DNase I; 0.5 mg/ml), and 1 × protease inhibitor (MCE). The entire purification procedures were performed at 4°C. After sonication on ice, the membrane fraction was solubilized at 4°C for 2 hours with lysis buffer supplemented with 1% (w/v) LMNG (Anatrace). After centrifugation at 48,000*g* for 45 min, the supernatant was collected and subjected to affinity chromatography with Strep-Tactin resin (IBA). The resin was then rinsed with wash buffer (buffer W) containing 25 mM tris (pH 8.0), 150 mM NaCl, 10% glycerol, and 0.04% GDN. The protein was eluted with buffer W supplemented with 5 mM D-desthiobiotin. After the removal of the C-terminal affinity tag with PreScission Protease, Derlin-1 was concentrated and further purified by size-exclusion chromatography using Superdex 200 Increase 10/300 GL (GE Healthcare) preequilibrated in buffer containing 25 mM tris (pH 8.0), 150 mM NaCl, and 0.02% GDN. The peak fractions were pooled and concentrated to approximately 1.5 mg/ml for cryosample preparation.

cryo-EM sample preparation and data collection

Three-microliter aliquots of the samples were applied to glow-discharged holey carbon grids (Quantifoil R1.2/1.3 Au, 300 mesh), and after 15-s incubation, the grids were blot for 2.5 s and rapidly plunged into liquid ethane cooled by liquid nitrogen, using a Vitrobot Mark IV (FEI) operated at 10°C and 100% humidity. The grids were imaged using a Titan Krios transmission electron microscope (FEI) operated at 300 kV, with the specimen maintained at liquid nitrogen temperatures. Images were automatically collected with EPU software (FEI) on a K3 camera (Gatan) operated in superresolution counting mode, placed at the end of a GIF Quantum energy filter (Gatan), functioning in zero–energy loss mode with a slit width of 15 eV. Data were typically collected at a nominal magnification of 105,000× (corresponding to a physical pixel size of 0.86 Å), with a defocus range between −1.0 and −2.5 μm. The dose rate was set to ~18.2 electrons/$Å^2$ per s, and the total exposure time was 2.7 s, resulting in a total dose of 50 electrons/$Å^2$, fractionated into 32 frames.

cryo-EM data processing

A total of 15,752 cryo-EM images were collected, and motion correction was performed on the dose-fractioned image stacks using MotionCor2 with dose weighting (*38*, *39*). The contrast transfer function (CTF) parameters of each image were determined with

Table 1. Cryo-EM data collection, processing, model refinement, and validation statistics. RMS, root mean square.

Data collection and processing	
Microscope	Titan Krios G3i
Detector	Gatan K3 camera
Nominal magnification	105,000×
Voltage (kV)	300
Energy filter slit width	15 eV
Pixel size (Å per pixel)	0.86
Electron exposure (e^-/Å^2)	50
Defocus range (μm)	−1.0 to 2.5
Symmetry imposed	C2
Number of movies	15,752
Final particle numbers	71,761
Map resolution (Å)	3.85
Fourier shell correlation (FSC) threshold	0.143
Map sharpening B factor (Å^2)	−162.4
Model building and refinement	
Model composition	
Protein residues	776
Ligands	0
RMS deviations from ideal	
Bond lengths (Å)	0.009
Bond angles (°)	1.328
Validation	
MolProbity score	2.06
Clashscore	6.93
Rotamer outliers (%)	1.10
Ramachandran plot	
Favored (%)	85.68
Allowed (%)	14.32
Outlier (%)	0.00

Gctf (*40*), and automatic particle picking was carried out using Gautomatch v0.56 (www2.mrc-lmb.cam.ac.uk/research/locally-developed-software/zhang-software/#gauto) on the basis of templates generated from a few hundred manually picked particles. Subsequent image processing steps were performed with RELION-3 (*41*) and cryoSPARC (*42*). An overview of the data processing procedure is shown in figs. S2 and S3. The particles were first extracted with 2× binning (1.72 Å per pixel), and junk particles were removed by two rounds of 2D classifications. The remaining particles were subjected to 3D classification with C4 symmetry imposed, using an initial reference generated by cryoSPARC. The particles corresponding to the best class were reextracted without binning (0.86 Å per pixel) and further processed with 3D autorefinement and solvent-masked postprocessing, which generated a cryo-EM density map with an overall resolution of 4.7 Å. Bayesian polishing and CTF refinement were then applied, which improved the overall resolution to 4.4 Å. However, further analysis of 2D class averages suggested a C2 symmetry rather than C4 symmetry might apply. After 3D classification with C2 symmetry imposed, particles corresponding to the best class were reextracted without binning and further processed with 3D autorefinement, Bayesian polishing, and CTF refinement, resulting in an overall resolution of 4.5 Å. To further improve the resolution and the map quality, 3D classification without alignment was performed (K = 6 and T = 12), yielding a total of 71,761 particles, which generated a reconstruction with an overall resolution of 4.1 Å after 3D autorefinement, Bayesian polishing, and CTF refinement. Alternatively, the subset of 71,761 particles was imported into cryoSPARC followed by a nonuniform refinement with C2 symmetry and an adaptive solvent mask (*43*) and thereby yielded a map with an overall resolution of 3.8 Å. Local resolution estimation was performed by cryoSPARC, and all the resolutions were estimated with the gold-standard Fourier shell correlation of 0.143 criteria with high-resolution noise substitution (*44*–*46*).

Model building and refinement

The cryo-EM structure model of yeast Der1 (PDB ID 6VJZ) was used as reference for initial model building using Phenix (*47*). The initial model was then docked into the electron density map using Chimera (*48*), followed by iterative manual adjustment in COOT (*49*) and real-space refinement using Phenix.

Cell culture, transfections, affinity capture, and immunoblotting

HEK293T cells were cultured in Dulbecco's modified Eagle's medium (Sigma-Aldrich) supplemented with 10% fetal bovine serum (ExCell Bio, catalog no. FSP500, lot no.11F364) at 37°C with 5% CO_2. Cells were cotransfected with 4 μg of pcDNA3.4-NHK with a C-terminal flag tag and 4 μg of modified pcDNA3.4–Derlin-1 with a C-terminal twin-strep tag, encoding wild type or mutants or the empty vector per 6-cm dish using Lipofectamine 2000 (Thermo Fisher Scientific), according to the manufacturer's instruction, and incubated for 6 hours at 37°C. Subsequently, transfection media were replaced with fresh culture media, and cells were incubated at 37°C for 48 hours before harvest. HEK293T cells were collected by centrifugation and washed with phosphate-buffered saline (PBS). The entire purification process was carried out at 4°C. Cells were resuspended in 2 ml of buffer containing 20 mM Hepes (pH 7.5), 150 mM NaCl, 10% glycerol, 5 mM $MgCl_2$, DNase I (0.5 mg/ml), and 1× protease inhibitor (MCE) and then solubilized at 4°C for 4 hours with 2% (w/v) digitonin (Sigma-Aldrich). After centrifugation at 21,000*g* for 40 min, the supernatant was collected and applied to Strep-Tactin XT–coated magnetic beads (IBA). The beads were rinsed with wash buffer containing 20 mM Hepes (pH 7.5), 150 mM NaCl, 10% glycerol, and 0.06% digitonin. The magnetic beads with Strep-tagged proteins were resuspended in loading buffer and then were run on uniform SDS–polyacrylamide gel electrophoresis (PAGE) gels before transferred to polyvinylidene difluoride membranes for immunoblotting.

In-membrane cross-linking of hDERL1 proteins

The cDNAs for human DERL1 or its mutants were cloned into a modified pcDNA3.4 plasmids, transfected into HEK293T cells using Lipofectamine 2000, according to the manufacturer's instruction, and incubated for 6 hours at 37°C. Subsequently, transfection media were replaced with fresh culture media, and cells were incubated at 37°C for 48 hours before harvest. HEK293T cells were collected by centrifugation and washed with PBS. Cells were resuspended in

buffer containing PBS (pH 7.2) and 1× protease inhibitor (MCE). After sonication on ice, 20 μl of membrane fraction was mixed with 1 mM 1,11-bismaleimido-triethyleneglycol (Thermo Fisher Scientific) or dimethyl sulfoxide as solvent control. Cross-linking reactions were performed on ice for 2 hours and then quenched on ice for 30 min with 50 mM dithiothreitol. The samples were subjected to SDS-PAGE and then immunoblotting with antibody to hDERL1.

Antibodies

The following antibodies were used: anti-NHK [SERPINA1 rabbit polyclonal antibody (pAb); ABclonal, A1015], anti–Derlin-1 (Derlin-1 rabbit pAb; Abcam, ab176732), anti–glyceraldehyde-3-phosphate dehydrogenase (GAPDH) (GAPDH mouse monoclonal antibody; ProteinTech, 60004-1-Ig).

SUPPLEMENTARY MATERIALS

Supplementary material for this article is available at http://advances.sciencemag.org/cgi/content/full/7/10/eabe8591/DC1

View/request a protocol for this paper from *Bio-protocol*.

REFERENCES AND NOTES

1. E. D. Werner, J. L. Brodsky, A. A. McCracken, Proteasome-dependent endoplasmic reticulum-associated protein degradation: An unconventional route to a familiar fate. *Proc. Natl. Acad. Sci. U.S.A.* **93**, 13797–13801 (1996).
2. D. N. Hebert, M. Molinari, In and out of the ER: Protein folding, quality control, degradation, and related human diseases. *Physiol. Rev.* **87**, 1377–1408 (2007).
3. S. S. Vembar, J. L. Brodsky, One step at a time: Endoplasmic reticulum-associated degradation. *Nat. Rev. Mol. Cell Biol.* **9**, 944–957 (2008).
4. G. D. Watts, J. Wymer, M. J. Kovach, S. G. Mehta, S. Mumm, D. Darvish, A. Pestronk, M. P. Whyte, V. E. Kimonis, Inclusion body myopathy associated with Paget disease of bone and frontotemporal dementia is caused by mutant valosin-containing protein. *Nat. Genet.* **36**, 377–381 (2004).
5. K. Nakatsukasa, G. Huyer, S. Michaelis, J. L. Brodsky, Dissecting the ER-associated degradation of a misfolded polytopic membrane protein. *Cell* **132**, 101–112 (2008).
6. E. J. Wiertz, D. Tortorella, M. Bogyo, J. Yu, W. Mothes, T. R. Jones, T. A. Rapoport, H. L. Ploegh, Sec61-mediated transfer of a membrane protein from the endoplasmic reticulum to the proteasome for destruction. *Nature* **384**, 432–438 (1996).
7. S. Schoebel, W. Mi, A. Stein, S. Ovchinnikov, R. Pavlovicz, F. DiMaio, D. Baker, M. G. Chambers, H. Su, D. Li, T. A. Rapoport, M. Liao, Cryo-EM structure of the protein-conducting ERAD channel Hrd1 in complex with Hrd3. *Nature* **548**, 352–355 (2017).
8. Y. Ye, Y. Shibata, C. Yun, D. Ron, T. A. Rapoport, A membrane protein complex mediates retro-translocation from the ER lumen into the cytosol. *Nature* **429**, 841–847 (2004).
9. B. N. Lilley, H. L. Ploegh, A membrane protein required for dislocation of misfolded proteins from the ER. *Nature* **429**, 834–840 (2004).
10. X. Wu, M. Siggel, S. Ovchinnikov, W. Mi, V. Svetlov, E. Nudler, M. Liao, G. Hummer, T. A. Rapoport, Structural basis of ER-associated protein degradation mediated by the Hrd1 ubiquitin ligase complex. *Science* **368**, eaaz2449 (2020).
11. M. K. Lemberg, J. Menendez, A. Misik, M. Garcia, C. M. Koth, M. Freeman, Mechanism of intramembrane proteolysis investigated with purified rhomboid proteases. *EMBO J.* **24**, 464–472 (2004).
12. E. J. Greenblatt, J. A. Olzmann, R. R. Kopito, Derlin-1 is a rhomboid pseudoprotease required for the dislocation of mutant α-1 antitrypsin from the endoplasmic reticulum. *Nat. Struct. Mol. Biol.* **18**, 1147–1152 (2011).
13. B. K. Sato, R. Y. Hampton, Yeast Derlin Dfm1 interacts with Cdc48 and functions in ER homeostasis. *Yeast* **23**, 1053–1064 (2006).
14. R. Hitt, D. H. Wolf, Der1p, a protein required for degradation of malfolded soluble proteins of the endoplasmic reticulum: Topology and Der1-like proteins. *FEMS Yeast Res.* **4**, 721–729 (2004).
15. F. Sun, R. Zhang, X. Gong, X. Geng, P. F. Drain, R. A. Frizzell, Derlin-1 promotes the efficient degradation of the cystic fibrosis transmembrane conductance regulator (CFTR) and CFTR folding mutants. *J. Biol. Chem.* **281**, 36856–36863 (2006).
16. M. Knop, A. Finger, T. Braun, K. Hellmuth, D. H. Wolf, Der1, a novel protein specifically required for endoplasmic reticulum degradation in yeast. *EMBO J.* **15**, 753–763 (1996).
17. C. Schuberth, A. Buchberger, Membrane-bound Ubx2 recruits Cdc48 to ubiquitin ligases and their substrates to ensure efficient ER-associated protein degradation. *Nat. Cell Biol.* **7**, 999–1006 (2005).
18. J. J. Lim, Y. Lee, S. Y. Yoon, T. T. Ly, J. Y. Kang, H. S. Youn, J. Y. An, J. G. Lee, K. R. Park, T. G. Kim, J. K. Yang, Y. Jun, S. H. Eom, Structural insights into the interaction of human p97 N-terminal domain and SHP motif in Derlin-1 rhomboid pseudoprotease. *FEBS Lett.* **590**, 4402–4413 (2016).
19. S. Neal, P. A. Jaeger, S. H. Duttke, C. Benner, C. K. Glass, T. Ideker, R. Y. Hampton, The Dfm1 Derlin is required for ERAD retrotranslocation of integral membrane proteins. *Mol. Cell* **69**, 306–320.e4 (2018).
20. A. Stolz, R. S. Schweizer, A. Schafer, D. H. Wolf, Dfm1 forms distinct complexes with Cdc48 and the ER ubiquitin ligases and is required for ERAD. *Traffic* **11**, 1363–1369 (2010).
21. Y. Ye, Y. Shibata, M. Kikkert, S. van Voorden, E. Wiertz, T. A. Rapoport, Recruitment of the p97 ATPase and ubiquitin ligases to the site of retrotranslocation at the endoplasmic reticulum membrane. *Proc. Natl. Acad. Sci. U.S.A.* **102**, 14132–14138 (2005).
22. O. S. Smart, J. G. Neduvelil, X. Wang, B. A. Wallace, M. S. Sansom, HOLE: A program for the analysis of the pore dimensions of ion channel structural models. *J. Mol. Graph.* **14**, 354–360 (1996).
23. K. Gotfryd, A. F. Mosca, J. W. Missel, S. F. Truelsen, K. Wang, M. Spulber, S. Krabbe, C. Helix-Nielsen, U. Laforenza, G. Soveral, P. A. Pedersen, P. Gourdon, Human adipose glycerol flux is regulated by a pH gate in AQP10. *Nat. Commun.* **9**, 4749 (2018).
24. L. Zhang, D. Yao, Y. Xia, F. Zhou, Q. Zhang, Q. Wang, A. Qin, J. Zhao, D. Li, Y. Li, L. Zhou, Y. Cao, The structural basis for glycerol permeation by human AQP7. *Sci. Bull.*, (2020).
25. Y. Wang, Y. Ha, Open-cap conformation of intramembrane protease GlpG. *Proc. Natl. Acad. Sci. U.S.A.* **104**, 2098–2102 (2007).
26. C. L. Brooks, C. Lazareno-Saez, J. S. Lamoureux, M. W. Mak, M. J. Lemieux, Insights into substrate gating in H. influenzae rhomboid. *J. Mol. Biol.* **407**, 687–697 (2011).
27. Y. Wang, Y. Zhang, Y. Ha, Crystal structure of a rhomboid family intramembrane protease. *Nature* **444**, 179–180 (2006).
28. S. Cho, R. P. Baker, M. Ji, S. Urban, Ten catalytic snapshots of rhomboid intramembrane proteolysis from gate opening to peptide release. *Nat. Struct. Mol. Biol.* **26**, 910–918 (2019).
29. Z. Wu, N. Yan, L. Feng, A. Oberstein, H. Yan, R. P. Baker, L. Gu, P. D. Jeffrey, S. Urban, Y. Shi, Structural analysis of a rhomboid family intramembrane protease reveals a gating mechanism for substrate entry. *Nat. Struct. Mol. Biol.* **13**, 1084–1091 (2006).
30. T. A. Rapoport, Protein translocation across the eukaryotic endoplasmic reticulum and bacterial plasma membranes. *Nature* **450**, 663–669 (2007).
31. K. Romisch, A case for Sec61 channel involvement in ERAD. *Trends Biochem. Sci.* **42**, 171–179 (2017).
32. P. Carvalho, V. Goder, T. A. Rapoport, Distinct ubiquitin-ligase complexes define convergent pathways for the degradation of ER proteins. *Cell* **126**, 361–373 (2006).
33. R. Y. Hampton, R. G. Gardner, J. Rine, Role of 26S proteasome and HRD genes in the degradation of 3-hydroxy-3-methylglutaryl-CoA reductase, an integral endoplasmic reticulum membrane protein. *Mol. Biol. Cell* **7**, 2029–2044 (1996).
34. R. D. Baldridge, T. A. Rapoport, Autoubiquitination of the Hrd1 ligase triggers protein retrotranslocation in ERAD. *Cell* **166**, 394–407 (2016).
35. V. Vasic, N. Denkert, C. C. Schmidt, D. Riedel, A. Stein, M. Meinecke, Hrd1 forms the retrotranslocation pore regulated by auto-ubiquitination and binding of misfolded proteins. *Nat. Cell Biol.* **22**, 274–281 (2020).
36. M. Suzuki, T. Otsuka, Y. Ohsaki, J. Cheng, T. Taniguchi, H. Hashimoto, H. Taniguchi, T. Fujimoto, Derlin-1 and UBXD8 are engaged in dislocation and degradation of lipidated ApoB-100 at lipid droplets. *Mol. Biol. Cell* **23**, 800–810 (2012).
37. H. You, Y. Ge, J. Zhang, Y. Cao, J. Xing, D. Su, Y. Huang, M. Li, S. Qu, F. Sun, X. Liang, Derlin-1 promotes ubiquitylation and degradation of the epithelial Na^+ channel, ENaC. *ENaC. J. Cell Sci.* **130**, 1027–1036 (2017).
38. T. Grant, N. Grigorieff, Measuring the optimal exposure for single particle cryo-EM using a 2.6 A reconstruction of rotavirus VP6. *eLife* **4**, e06980 (2015).
39. S. Q. Zheng, E. Palovcak, J. P. Armache, K. A. Verba, Y. Cheng, D. A. Agard, MotionCor2: Anisotropic correction of beam-induced motion for improved cryo-electron microscopy. *Nat. Methods* **14**, 331–332 (2017).
40. K. Zhang, Gctf: Real-time CTF determination and correction. *J. Struct. Biol.* **193**, 1–12 (2016).
41. J. Zivanov, T. Nakane, B. O. Forsberg, D. Kimanius, W. J. Hagen, E. Lindahl, S. H. Scheres, New tools for automated high-resolution cryo-EM structure determination in RELION-3. *eLife* **7**, e42166 (2018).
42. A. Punjani, J. L. Rubinstein, D. J. Fleet, M. A. Brubaker, cryoSPARC: Algorithms for rapid unsupervised cryo-EM structure determination. *Nat. Methods* **14**, 290–296 (2017).
43. A. Punjani, H. Zhang, D. J. Fleet, Non-uniform refinement: Adaptive regularization improves single-particle cryo-EM reconstruction. *Nat. Methods* **17**, 1214–1221 (2020).
44. P. B. Rosenthal, R. Henderson, Optimal determination of particle orientation, absolute hand, and contrast loss in single-particle electron cryomicroscopy. *J. Mol. Biol.* **333**, 721–745 (2003).

45. S. H. Scheres, S. Chen, Prevention of overfitting in cryo-EM structure determination. *Nat. Methods* **9**, 853–854 (2012).
46. S. Chen, G. McMullan, A. R. Faruqi, G. N. Murshudov, J. M. Short, S. H. Scheres, R. Henderson, High-resolution noise substitution to measure overfitting and validate resolution in 3D structure determination by single particle electron cryomicroscopy. *Ultramicroscopy* **135**, 24–35 (2013).
47. D. Liebschner, P. V. Afonine, M. L. Baker, G. Bunkoczi, V. B. Chen, T. I. Croll, B. Hintze, L. W. Hung, S. Jain, A. J. McCoy, N. W. Moriarty, R. D. Oeffner, B. K. Poon, M. G. Prisant, R. J. Read, J. S. Richardson, D. C. Richardson, M. D. Sammito, O. V. Sobolev, D. H. Stockwell, T. C. Terwilliger, A. G. Urzhumtsev, L. L. Videau, C. J. Williams, P. D. Adams, Macromolecular structure determination using x-rays, neutrons and electrons: Recent developments in Phenix. *Acta Crystallogr. D Struct. Biol.* **75**, 861–877 (2019).
48. E. F. Pettersen, T. D. Goddard, C. C. Huang, G. S. Couch, D. M. Greenblatt, E. C. Meng, T. E. Ferrin, UCSF Chimera–A visualization system for exploratory research and analysis. *J. Comput. Chem.* **25**, 1605–1612 (2004).
49. P. Emsley, B. Lohkamp, W. G. Scott, K. Cowtan, Features and development of Coot. *Acta Crystallogr. D Biol. Crystallogr.* **66**, 486–501 (2010).

Acknowledgments: We thank M. Zhou, M. Lei, X. Chen, Z. Zhang, A. Qin, and L. Wang for scientific discussion and R. Liao and M. Cao for assistance with the data analysis. We thank the staff members of the Electron Microscopy System and Mass Spectrometry System at Shanghai Institute of Precision Medicine for providing technical support and assistance in data collection. **Funding:** This work is supported by National Key Research and Development Program of China (2018YFC1004704 and 2017YFC1001303), National Natural Science Foundation of China (U1632132 and 31670849), SHIPM-pi fund no. JY201804 from Shanghai Institute of Precision Medicine, Shanghai Ninth People's Hospital, Shanghai Jiao Tong University School of Medicine. This work is also supported by Innovative Research Team of High-level Local Universities in Shanghai (SSMU-ZLCX20180600). **Author contributions:** Y.C. initiated the study. Y.C. and B.R. designed the research and wrote the paper. B.R., Q.W., and Y.J. performed the purification and EM sample preparation. B.R., S.L., Q.W., Y.S., and Y.X. collected and analyzed the data. B.R., S.L., D.Y., and Y.C. determined the structure. **Competing interests:** The authors declare that they have no competing interests. **Data and materials availability:** The coordinates are deposited at PDB with accession code: 7CZB. The cryo-EM map has been deposited in the Electron Microscopy Data Bank (EMDB) with accession code: EMD-30508. All data needed to evaluate the conclusions in the paper are present in the paper and/or the Supplementary Materials. Additional data related to this paper may be requested from the authors.

Submitted 18 September 2020
Accepted 19 January 2021
Published 3 March 2021
10.1126/sciadv.abe8591

Citation: B. Rao, S. Li, D. Yao, Q. Wang, Y. Xia, Y. Jia, Y. Shen, Y. Cao, The cryo-EM structure of an ERAD protein channel formed by tetrameric human Derlin-1. *Sci. Adv.* **7**, eabe8591 (2021).